Improving energy and visual performance in offices using building integrated perovskite-based solar cells: A case study in Southern Italy

Post-print version of the paper published in Applied Energy, Volume 205, 1 November 2017, Pages 834-846, doi: https://doi.org/10.1016/j.apenergy.2017.08.112

Improving energy and visual performance in offices using building integrated perovskite-based solar cells: a case study in Southern Italy

Alessandro Cannavale[a], Laura Ierardi[a], Maximilian Hörantner[b], Giles E. Eperon[c,d], Henry J. Snaith[b], Ubaldo Ayr[a] and Francesco Martellotta[a]*

a) Department of Civil Engineering and Architecture (DICAR), Politecnico di Bari, via Orabona 4, 70125 Bari (Italy)
b) Department of Physics, University of Oxford, Oxford, Parks Road, OX1 3PU, UK
c) Department of Chemistry, University of Washington, Seattle, WA 98105, USA
d) Cavendish Laboratory, JJ Thomson Avenue, Cambridge CB3 0HE, UK

Abstract

Building integration of innovative photovoltaic technologies, defined by high efficiency and optical properties allowing their use as a replacement of solar control films, offer new opportunities for energy saving. In order to estimate this potential under real world conditions, we have carried out simulations for this scenario based on an existing office building located in Bari (Italy). The building has a significant amount of transparent surfaces combined with transparent shades, while office layout corresponds to a typical Mediterranean configuration with several single/double offices (2.9 m by 6.6 m). We investigate the effect of the replacement of standard clear glass windows with new windows integrating perovskite-based semi-transparent photovoltaic modules, and the replacement of the original transparent shading system with high performance opaque perovskite-perovskite tandem cells. In particular, the attributes that were directly influenced by the proposed modifications were investigated in detail, including overall energy consumption for heating, air conditioning, and artificial lighting, evaluated against the overall energy yield given by building-integrated photovoltaic modules. Results showed that under ideal conditions (no obstructing buildings) yearly savings up to 18% could be obtained. In presence of nearby buildings savings dropped to 14%. Considering that fabrication costs for this technology are promisingly low and that this is currently the

only neutral colored semi-transparent photovoltaic, the above results are promising, particularly for buildings with large window-to-wall ratios.

1 Introduction

Energy use in residential and commercial buildings is responsible for a significant part of energy consumption worldwide. For instance, in the European Union, the share of final energy utilization due to tertiary sector (mainly buildings) reaches 42.6%. [1]

The urgent need of keeping the global temperature increase from climate change "well below 2 °C" pushed most nations to subscribe the COP21 agreement, aiming at a massive reduction of greenhouse gas (GHG) emissions. Moreover, the European Directive 2012/13/EU requires innovative design criteria for buildings to obtain very low yearly energy consumption in new constructions, as a combined effect of energy efficient design and use of renewable energy resources [2].

Effective integration of innovative renewable sources like photovoltaics (PV) in the design of building components is a key element to the success of energy demand minimization. Consequently, research in the field of Building Integration of Photovoltaics (BIPV) is now becoming more relevant and prevalent. PVs will probably represent the main innovative form of renewable energy allowing the transition of buildings' energy sources towards the imminent "smart grid" era.

Different from Building Adopted PV systems, where PV panels are simply attached on exterior parts of building envelopes (on rooftops or facades), BIPV systems represent architecturally relevant components. They are active energy-producing units requiring the complex fulfillment of multiple requirements (aesthetic, economic, structural, acoustic, thermal, etc.). [3,4] From this point of view, well established technologies such as monocrystalline (c-Si) and polycrystalline (p-Si) silicon PV modules, despite their high conversion efficiencies (η), equal to 20% and 15% respectively, are not suitable for building integration, due to being inherently rigid, opaque and flat [5,6]. However, it has been speculated that emerging technologies may even outperform c-Si cells in specific operation conditions: high temperatures or sub-optimal tilt angles [5].

Post-print version of the paper published in Applied Energy, Volume 205, 1 November 2017, Pages 834-846, doi: https://doi.org/10.1016/j.apenergy.2017.08.112

The tunable bandgap of some novel PV technologies can result in semitransparent components that may match the optical (and thermal) requirements underlying integration in architectural glazings. Much research activity in the emerging field of hybrid and organic PV is currently related to the development of semitransparent, color-tunable, flexible, lightweight, robust and easily-processable PV technologies. [7]

Among these technologies, low-cost, lightweight and flexible amorphous silicon semitransparent solar cells have already been reported [2], and several products are now available on the market. However, as clearly reported in the works by Zhang et al. [8], using commercial a-Si solar cells (η=5.9%, T_{vis}=0.15), by Lim et al. [9], using specifically designed cells (η=5.93%, T_{vis}=0.18), and by Chae et al. [10], these devices offer very low transparency and marked coloration.

Regarding newer technologies, 1.2 μm thick Cu(In,Ga)Se_2 (CIGS) semitransparent solar cells were reported, with a conversion efficiency of 5.6% [2]. TOrganic PVs represent another promising option, but their commercial uptake is still impeded by durability concerns, even though they use thin, flexible layers of organic light-harvesting molecules to generate power [11,12] and efficiencies close to the best reported (11.5%) can be attained for semi-transparent devices.

Dye sensitized cells (DSCs) [13] are of particular interest for BIPV for their inherent semitransparency, color tunability according to the dyes used, light weight and possible flexibility, though chemical degradation, leakage problems when using liquid electrolytes, and photochemical degradation of dyes and sealants still hamper their diffusion. De Rossi et al. [14] showed that flexible DSCs with specially formulated transparent electrolytes outperformed all other PV technologies, providing average power densities of 8.0 μW/cm^2 and 12.4% efficiencies under 200 lux compact fluorescent lamps.

However, the most promising emergent PV technology at the moment is represented by perovskite-based solar cells, consisting of hybrid organic-inorganic metal halides [15]. These materials enable accurate tuning of bandgaps between ~1.2 and 3eV[16–19]. Besides their impressive conversion efficiencies (up to 22%)[20], perovskite-based cells can be easily manipulated to obtain semi-transparency. A typical device consists of a

Post-print version of the paper published in Applied Energy, Volume 205, 1 November 2017, Pages 834-846, doi: https://doi.org/10.1016/j.apenergy.2017.08.112

perovskite layer sandwiched between electron and hole transporting materials, respectively in contact with anode and cathode. The perovskite is typically thick enough to absorb most incident light, resulting in a completely opaque device. Two main approaches have been reported to enhance transparency: making perovskite layers thinner, although a disadvantage of this option is that it provides brownish cells [21], or controlling the perovskite morphology so as to fabricate discontinuous micro-islands by tuning the physical parameters of the perovskite deposition process [22]. Such islands, when suitably designed, are invisible to the human eye and form neutral-tinted films, with minimal impact on the spectral properties of light passing through. Recently, Hörantner et al. [23] made significant advances in this architecture by blocking shunting paths between islands via deposition of a transparent, insulating octadecyl-siloxane molecular layer. Due to these attractive characteristics, highly transparent perovskites have already been integrated in photovoltachromic devices [24,25]

Integration of PV technologies into a building implies affecting its "passive" energetic behavior (in terms of energy balance), as well as occupants' comfort conditions, when the BIPV is applied to windows and similar elements. Compliance to regulations often imposes limits to the use of such technologies (e.g. the minimum acceptable glazing transmittance, in modern offices, lies in the range between 25% and 38% [26]). Relating to these restrictions, Zomer et al. [27] investigated the balance between aesthetics and performance in building integrated first generation photovoltaics, and Yang and Zou [28] investigated benefits and barriers to the diffusion of BIPV technologies. The manifold advantages and potentialities of BIPV technology were thoroughly investigated, such as the reduction of carbon emissions and social costs, environmental impact of constructions, significant reduction in land use for the generation of electricity and savings on electricity bills. They also highlighted that BIPV systems may result in a mere cost offset by replacing traditional building materials in architectural envelopes. As reported by Benemann et al. [6], compared to a standard glass facade or a structural glazing facade, BIPV silicon cells adds an additional cost of about 350-500 $/m^2. Several case studies have been reported for building-integrated a-Si cells. [29] Chatzipanagi et al. [30] presented the results of a demonstrative (BIPV) installation, finding that fully

Post-print version of the paper published in Applied Energy, Volume 205, 1 November 2017, Pages 834-846, doi: https://doi.org/10.1016/j.apenergy.2017.08.112

integrated modules exhibited higher temperatures. Integrated c-Si modules showed a lower energy yield than the integrated and ventilated a-Si/a-Si modules, for which the high operating temperatures proved to be beneficial. Peng et al. [31] constructed a simulation model to predict the energy performance and energy-saving potential of a ventilated photovoltaic double-skin facade in a Mediterranean climate zone, that was able to generate about 65 kWh electricity yearly, adopting a-Si semi-transparent PV modules, with low visible transmittance (T_{vis}=7% - unsuitable for office incorporation as mentioned above).

More recently, Chae et al. [10] suggested a procedure to evaluate the energy performance of buildings incorporating BIPVs, considering not only the electrical characteristics of PV cells, but also thermal and optical behavior and the consequent implications on building energy performance. They found that the maximum electric energy generation using a-Si:H cells could range from 22 kWh/m^2 per year to 45 kWh/m^2 per year, depending on several parameters including the type of PV cell, the site location and the exposure. Some of the authors already used a similar approach to assess the benefits deriving from building integration of photoelectrochromic technologies. [25,32,33]

BIPV technologies based on a-Si cells showed interesting results, particularly in terms of energy yield. However, as anticipated, they may be strongly limited by relatively low T_{vis} values combined with a markedly orange-brown coloration. Such limitations may now be overcome by means of perovskite cells which, as demonstrated in a preliminary study involving a single "typical" office room [34], offer two advantages if integrated into buildings. First, they produce an annual amount of power which is comparable to that obtained by using commercial a-Si cells. Moreover, due to being neutrally colored, they can also be used as a replacement for solar control films for glasses (used to attenuate irradiance for visual comfort), effectively shielding undesired solar gains and thus allowing energy saving and the achievement of higher levels of visual comfort indoors. Consequently, they are particularly effective when used in buildings with large windows-to-wall-ratio (WWR>33%). This is consistent with the results shown by Oliver et al. [35].

Post-print version of the paper published in Applied Energy, Volume 205, 1 November 2017, Pages 834-846, doi: https://doi.org/10.1016/j.apenergy.2017.08.112

Recent literature also demonstrated that production costs for perovskite modules are expected to be much lower than other competing technologies, increasing the probability of its future usage in the BIPV market.

In order to investigate the potential benefits of this cutting-edge technology, integration of some of the best performing (in terms of efficiency, transparency, and neutral coloration) perovskite-based PV cells [36] into a real building was studied. This offered a more complex and realistic case than the simple office room investigated in [38], thus allowing a thorough analysis of its implications on the energy balance of a whole building, also including adverse effects such as those due to shading by surroundings. The case study is an existing office building located in Bari (Southern Italy) which can be considered as a paradigm of tertiary buildings adopted in Mediterranean climates (with large transparent surfaces combined with shades, office layout with several single/double offices covering an average area of 20-40 m^2).

Results, as described in detail later, confirm that the use of semi-transparent perovskite cells for glazings is certainly convenient for Southern and non-obstructed windows. Use of PV shades in addition reduced the energy yield of the windows, but largely compensated for that loss, also allowing differentiated orientation of PV surfaces so to have a more uniform output throughout the year.

2 Methods

2.1 Characterization of building-integrated photovoltaic technologies employed in the study

Two perovskite-based photovoltaic cells were used as model modules in this study. The neutral coloured semi-transparent perovskite solar cell devices used for glazings were thoroughly described by Hörantner et al. [23] In summary, these cells are fabricated by the coating of a compact TiO_2 n-type layer followed by dewetted perovskite islands on clean FTO. Shunt-blocking layers comprised of octadecyl-trichloro silane were additionally applied to improve the device performance before the hole transporting layer spiro-OMeTAD was deposited. A flexible Nickel micro grid was laminated to act as a transparent hole conducting electrode.

Post-print version of the paper published in Applied Energy, Volume 205, 1 November 2017, Pages 834-846, doi: https://doi.org/10.1016/j.apenergy.2017.08.112

The high transparency and neutral coloration of the perovskite-based cell is shown in Fig. 1. The high transmittance observed throughout the visible range are the main attraction of this novel technology. Starting from data measured in laboratory cells, visible transmittance was calculated according to the European Standard EN410, which specifies methods of determining the luminous and solar characteristics of glazing in buildings.

The performance of these cells, used as the basis of the reported simulations, is summarized in Table 1.

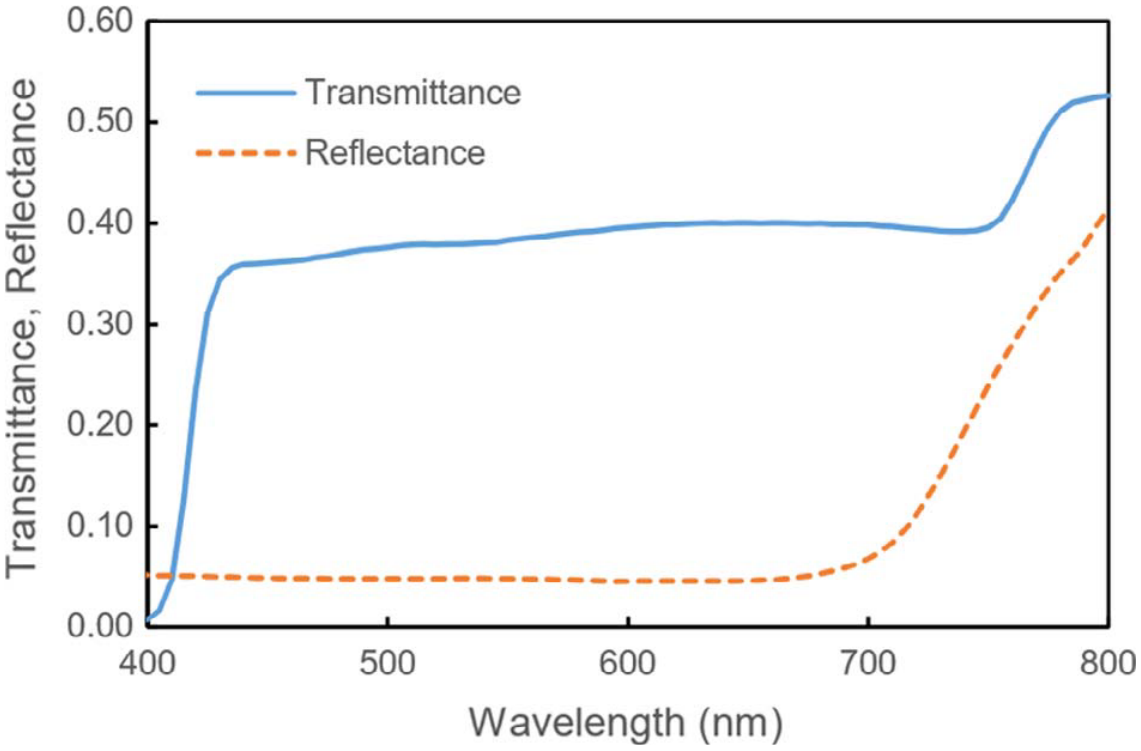

Fig. 1. *Total transmittance and reflectance spectrum of semi-transparent solar cell, measured with UV-vis spectrophotometer. Transmittance reproduced with permission from ref [xx].*

Table 1
Photovoltaic and optical parameters of perovskite solar cells used in the study.

	Light intensity [W/m^2]	*Short-circuit current (Jsc) [mA/cm^2]*	*Fill factor (FF)*	*Open circuit voltage (Voc) [V]*	*Conversion efficiency (η) [%]*	*Visible transmittance (Tvis) [%]*
Semitransparent cells	1000	11.0	0.65	0.95	6.6	42.4
1 cm^2 low gap subcell (filtered by wide gap)	1000	5.7	0.73	0.72	3.0	-

Post-print version of the paper published in Applied Energy, Volume 205, 1 November 2017, Pages 834-846, doi: https://doi.org/10.1016/j.apenergy.2017.08.112

1 cm^2 wide gap subcell	1000	19.3	0.65	1.08	13.0	-
1 cm^2 4T Tandem	1000	-	-	-	16.0	0

In addition to the semi-transparent device, an opaque planar heterojunction cell was also considered for this work. We chose a recently reported perovskite-perovskite 4-terminal tandem cell with matched bandgaps, exploiting an infrared-absorbing 1.2 eV band-gap perovskite (achieving 14.8% conversion efficiency) and a wider band-gap perovskite, so as to obtain an open circuit voltage as high as 1.71 V, Excellent stability and an overall conversion efficiency of 20.3% for small areas.[36] The photovoltaic conversion efficiency observed in larger devices (16.0% for an active area of 1 cm^2) was adopted for our simulations reported hereafter.

2.2 Case study description and proposed modifications

The case study assumed as a reference for the analysis is an office building located in the city of Bari, Apulia, on the east coast of southern Italy. The building is part of the headquarters of the Regional Departments of Apulia and is located in a suburban area, with low building density and limited interaction with nearby surroundings. Its high exposure to sunlight, its location and the significant proportion of transparent surfaces comprising its envelope made this building ideally suited to the purpose of the present study.

The building (Fig. 2) has a rectangular ground plan (measuring 80 m by 44 m), symmetrical along the axis of the short edge. With a height of about 12 m, it consists of three stories above ground, where all the office rooms are located, and a basement level with no offices.

The long axis of the building has an East-West orientation. Consequently, the largest facades have South and North exposure. A wide corridor with a glass ceiling crosses the building in its full height; running along the short axis of the ground plan, it divides the building into two blocks and links them at the same time. Each of the blocks has an internal patio providing fresh air and sunlight to office rooms with no exposure on the main facades.

Post-print version of the paper published in Applied Energy, Volume 205, 1 November 2017, Pages 834-846, doi: https://doi.org/10.1016/j.apenergy.2017.08.112

The reinforced concrete structure of the building allows a free layout: toilets and archives are bounded by brick walls, while the other partitions are movable, metallic sandwich panels, so that they can be easily placed in different positions to adapt the size of rooms to specific requirements, if necessary. All of this information is relevant to this study as architectural dimensions will affect the amount of shading needed. In the default state, the typical office rooms measure 2.9 m by 5.5 m or 2.9 m by 6.6 m. The net height of rooms and corridors is 3.55 m on the ground floor and 2.70 m on the first and second floors.

The building has a mechanical ventilation system and an air-conditioning system that uses both air and refrigerant as working fluids. The thermo-refrigerating station is in the basement and the pipe distribution system supplies fan-coil units in the office rooms. The whole system is electrically powered.

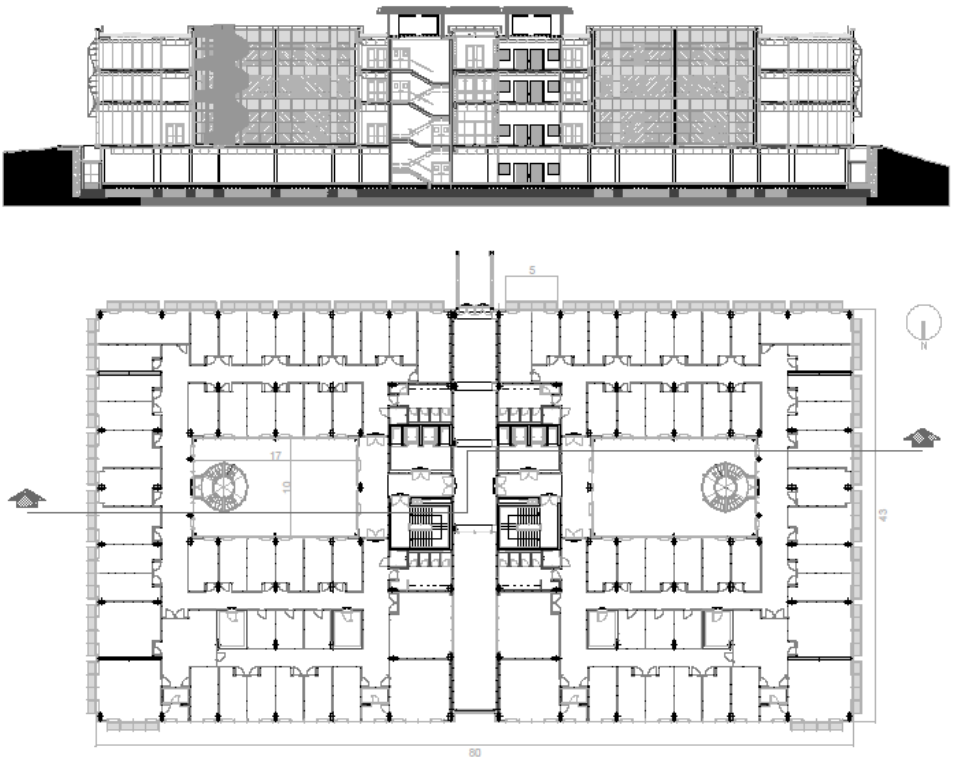

Fig. 2. *Ground plan of the first floor and cross-section of the investigated building*

Post-print version of the paper published in Applied Energy, Volume 205, 1 November 2017, Pages 834-846, doi: https://doi.org/10.1016/j.apenergy.2017.08.112

Fig. 3. *North and South façades of the building in its present state*

The building envelope (Fig. 3) is mainly made of glass, since on each façade the wide windows have nearly the same height as the corresponding office rooms. The total glazed surface area is 1715 m^2. The intersection between the floor and the external walls is covered by aluminum panels filled with thermal insulating material.

The double-glazed windows have hopper-type openings and simple aluminum frames. Three sides of the building and the corner offices on the north wall are provided with an external solar shading system consisting of static glass shelves, placed horizontally and held up by a metallic framework.

Here, to investigate the potential advantages of building integration of cutting-edge PV technologies, the following retrofitting options were considered.

- Replacing existing glazing (excluding North facing elements and those in the patios) with semi-transparent (T_{vis}=42.4%) perovskite based PV film [23,38] having 6% efficiency (STC);
- Replacing existing shades with a those made of opaque perovskite-perovskite tandem PV cells [36], having 16% efficiency (STC);
- A combination of both the above options.

As at this stage we wanted to investigate only the implications of using BIPV technologies on the energy balance of the building, we assumed as a reference condition that windows had had thermal performances complying with National regulations, and that this value was kept constant under all the simulations. For this reason, the original metallic frame

Post-print version of the paper published in Applied Energy, Volume 205, 1 November 2017, Pages 834-846, doi: https://doi.org/10.1016/j.apenergy.2017.08.112

was replaced by a PVC frame and the cavity between the glass surfaces was filled with Krypton gas. The facade layout was kept in its original setting. The glass panes of the reference (Clear Glass) window were chosen from the wide range of glazings contained in the International Glazing Database (IGDB), a comprehensive international glazing layer database compiled by NFRC [37]. With reference to the PV glass, its measured optical properties (shown in Fig. 1), combined with the emissivity (measured using the indirect approach proposed by Avdelidis et al. [38] and equal to 0.83), were used as input for the LBNL Optics and Window tools [REF]. This new layer was used to replace the external pane, and the resulting properties, calculated with the previously mentioned tools, were given in Table 2. Such data were subsequently imported into DesignBuilder to be used in the energy balance analysis.

The opaque envelope elements were modeled as white aluminum and zinc sheets with, in between, a double layer of extruded polystyrene and an air gap, for a total thickness of 0.25 m. The U-value assumed for the panels was 0.283 W/m^{2}K. For shades, a single 80 cm deep pane was assumed to be mounted on the top of each window, with its transparency set to 0.80 under reference conditions, and to 0 when PV cells were used. Table 3 summarizes the acronyms and main features of each investigated scenario.

Table 2
Glazing features as modeled for the analysis and calculated using LBNL Optics and Window 7.5

Name	Composition	U-Value (W/m^{2}K)	SHGC	T_{vis}	T_{Sol}
Clear Glass	Low-E pane "Pilkington K glass" 6mm Gap: Krypton 13 mm Clear glass pane "Pilkington Optifloat" 6 mm	1.573	0.674	0.726	0.550
PV Glass	Low-E pane "Pilkington K glass" 6 mm Gap: Krypton 13 mm Perovskite film on clear glass	1.571	0.422	0.350	0.292

Table 3
Summary of the cases under investigation and their relative acronyms

Acronym	Description
CG	Reference building, with clear glass windows with improved thermal performance (low-e)

Post-print version of the paper published in Applied Energy, Volume 205, 1 November 2017, Pages 834-846, doi: https://doi.org/10.1016/j.apenergy.2017.08.112

CG_S	Same as CG, with transparent shades (single pane 0.8 m deep, mounted on top of each window)
PV	Same as CG, with additional application of semi-transparent PV film to glazing
CG_SPV	Same as CG_S, but with opaque shades made of perovskite tandem PV cells
PV_SPV	Same as PV, with additional opaque shades made of perovskite tandem PV cells

2.3 Building simulation: energy balance

DesignBuilder software was used for modeling and analyzing the behavior of the case study in terms of energy consumption for heating and cooling. This tool enables easy creation of the building geometrical model handling of surface materials, occupancy and technical equipment, in order to run thermal simulations using the EnergyPlus simulation engine. The modeling process hence resulted in an accurate reproduction of the building in its main features (Fig. 4). Non-insulated mobile partitions were removed because their influence on heat flows was considered negligible. The interior walls not separating rooms were removed. The basement, which has no windows, is not relevant to the objectives of this study and thus was modeled as a simple empty story aimed at separating the lower occupied floor from the ground. These simplifications should not significantly affect the results in terms of heat exchange between spaces at different temperatures or between the building's interior and the outside.

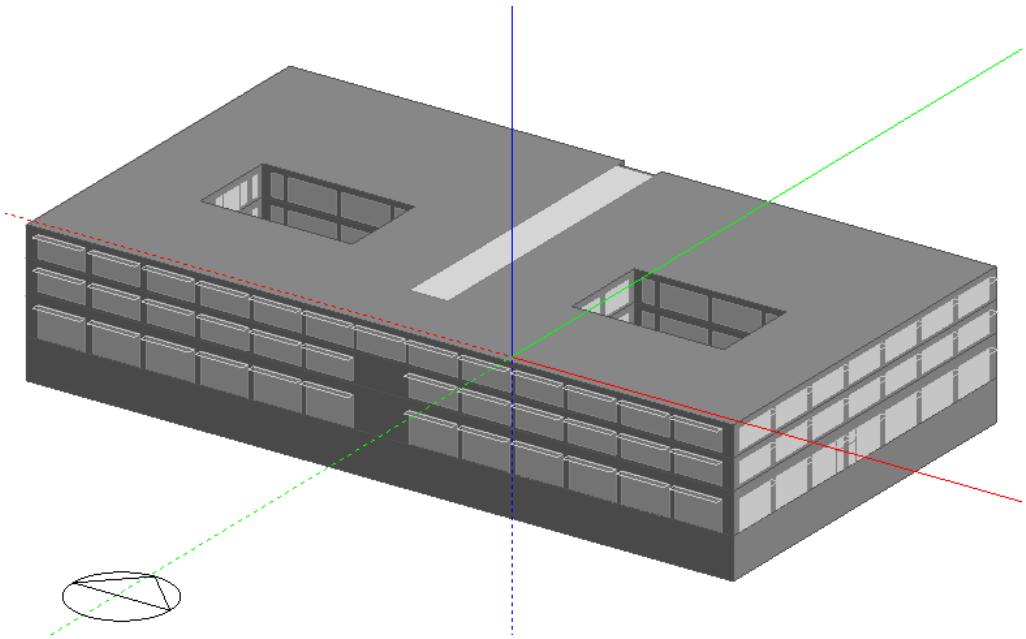

Post-print version of the paper published in Applied Energy, Volume 205, 1 November 2017, Pages 834-846, doi: https://doi.org/10.1016/j.apenergy.2017.08.112

Fig. 4. *3D Model of the building as modelled in DesignBuilder*

A major point when using simulation tools like DesignBuilder is the careful definition of the input data, as they determine the quality of the results. Consequently, occupancy schedules, based on actual use habits, were carefully adhered to, together with the number of users, the type of indoor activity, the structure of the typical working week and the heat gains due to office equipment. Cooling and heating set-point temperatures were also defined (Table 4). In this way, an environmental control device automatically turns on and off the air-conditioning system based on indoor temperatures. Heating and cooling are activated during working hours and the system, for the sake of simplicity, is assumed to be electrically powered with a COP of 3 (independent of heating/cooling mode). During unoccupied periods the system turns on only under "extreme" circumstances, according to the setback setpoint temperatures, to prevent the building becoming too cold or too hot and to reduce startup heating or cooling loads. A summary of the above mentioned settings is given in Table 4. Year-round simulations were finally run on a hourly basis to calculate the annual energy consumption for air-conditioning for each of the investigated scenarios.

Table 4
HVAC and occupancy parameters for DesignBuilder simulations.

Workday	*Work week*	*Occupancy density (people/m²)*	*Computer gains (W/m²)*	*Heating setpoint temperature [°C]*	*Heating setback temperature [°C]*	*Cooling setpoint temperature [°C]*	*Cooling setback temperature [°C]*
8.00 - 18.00	Mon -Fri	0.1	25	20	14	26	30

To allow possible comparisons of results referred to different locations, weather data taken from a large and homogeneous dataset are preferred. Consequently, the IWEC2 (International Weather for Energy Calculations) database developed by ASHRAE within the Research Project RP-1477, "Development of 3012 Typical Year Weather Files for International Locations," [39] was used. The thermal analysis was carried out using the climate data for Bari/Palese Macchie.

Calculations of the energy yield of the PV system were carried out according to a different approach. In fact, DesignBuilder/EnergyPlus is not capable of accounting for the

Post-print version of the paper published in Applied Energy, Volume 205, 1 November 2017, Pages 834-846, doi: https://doi.org/10.1016/j.apenergy.2017.08.112

dependence between radiation intensity and efficiency for the specific case of perovskite cells. In fact, this type of cells is characterized by an apparently linear dependence of efficiency on radiation intensity [34],[40]. None of the PV models embedded in the DesignBuilder/EnergyPlus platform reflects this behavior and, consequently, a hybrid approach was used here.

The DesignBuilder model was exported into EnergyPlus v. 8.6 [41], in order to take advantage of its more detailed output in terms of yearly exterior surface irradiation and surface temperature. For each window the overall incident solar radiation rate per area was obtained for each timestep (every hour). Considering the linear relationship between efficiency and radiation intensity, the corresponding PV cell efficiency was first calculated at the reference temperature of 25 °C. Then, the outside surface temperature was obtained for each window (assuming that, due to reduced thickness and high thermal conductivity, the outside surface temperature corresponded to the PV cell temperature). The cell efficiency was consequently corrected to consider the temperature effect, decreasing η by 0.3% every Celsius degree in excess of STC. [34] The same procedure was then repeated in presence of the shading system. In this case, the solar radiation rate and the surface temperature were calculated also for each shading device. For the sole purpose of estimating PV panel temperature, the Equivalent One-Diode model available in EnergyPlus was employed using the "Decoupled" heat transfer integration mode.

In all the above calculations, the effect of inverters, charge controllers, batteries, or maximum power point trackers was not included and the whole electrical part was supposed to operate under ideal conditions. Thus, the resulting values represent the upper limit of electricity production.

2.4 Building simulation: daylighting metrics

Daylighting analysis was necessary to calculate the influence of the proposed solutions on the energy consumption due to artificial lighting and, at the same time, calculate visual comfort metrics. Shading systems and semi-transparent glasses, although inducing increased costs due to artificial lighting, may conversely contribute to reduction of glare and over-illumination of indoor spaces. For the purpose of this analysis Daysim, a validated Radiance-based program, was used to predict indoor annual luminance and

Post-print version of the paper published in Applied Energy, Volume 205, 1 November 2017, Pages 834-846, doi: https://doi.org/10.1016/j.apenergy.2017.08.112

illuminance levels under real-sky conditions derived from the same statistical weather files [42]. Transparent materials (both photovoltaic and clear glass) were simulated through the "glass algorithm" which simulates glass as a special dielectric, accounting for the angular dependence of visual and solar transmission. The general algorithm takes into account the material's refraction, usually set at 1.52, the incidence angle of solar radiation, and the inter-reflections between the two surfaces of the panel. The only input variable is the transmissivity, typically used in radiance-based simulations, which is 1.09 times the visible transmittance, according to a simplified equation given by Jacobs [43]. Starting from glazing composition given in Table 2, this value was calculated and set equal to 0.791 for the "clear glass" (CG) configuration, and to 0.381 for the "photovoltaic glass" (PV) configuration.

Useful Daylight Illuminance (UDI) parameter, developed by Nabil et al. [44,45], was used to analyze light distribution inside the space throughout the year. It is defined as the percentage of time in which the illuminance falls within a range of values considered comfortable by the users. According to previous literature reviews on occupants' preferences and behaviors [44], a range of 100–2000 lx has been considered suitable for the current project. Daylight illuminances less than 100 lx are generally considered insufficient, whereas daylight illuminances higher than 2000 lx are likely to produce visual or thermal discomfort. Thus, low $UDI_{100\text{-}2000}$ is normally associated with zones very close to windows (over-illuminated), or very far from it (under-illuminated).

To evaluate glare risk, Daylight Glare Probability (DGP), developed by Wienold and Christoffersen [46] was used. According to Mardaljevic et al. [47], three classes of environment can be defined according to the value of DGP: "imperceptible" glare (DGP < 0.35 for 95% of the occupied time); "perceptible" glare (0.35<DGP < 0.40 for 95% of the occupied time); "disturbing" (0.40<DGP < 0.45 for 95% of the occupied time).

Considering the extent of the building under investigation, calculations were limited to two reference rooms. The small room is 2.90 m by 6.60 m, and the large room is 5.80 m by 6.60 m, with a height of 3.55 m at ground floor, and 2.70 m above. For this analysis only the lower height option of 2.70 m was considered, as providing more conservative results. A reference grid of illuminance sensors, made of 72 surveying points and set up

Post-print version of the paper published in Applied Energy, Volume 205, 1 November 2017, Pages 834-846, doi: https://doi.org/10.1016/j.apenergy.2017.08.112

at 85 cm above the floor level, corresponding to the ideal height of a workspace, was included in each room. The view point for DGP calculation was placed at a distance of 2 m from the window and at a height of 1.1 m above the floor level, representing the position of a typical seated user. To maximize the glare, the viewpoint was aimed at the corner with the highest luminance gradient. As required for the calculation of DGP, a view angle of 180° was considered (corresponding to a circular fisheye lens).

All the analyses were carried out for an entire year with reference to working hours only (from 8:00 AM to 6:00 PM), Monday to Friday. As the aim of these indoor natural illuminance levels calculations is to compare the effect of photovoltaic windows against traditional clear ones, standard material properties, included in Table 5, were adopted for the interior surfaces.

As discussed in Sec. 2.2, two glazing typologies were adopted in the analyses: a clear glass (CG), and a perovskite-based photovoltaic (PV) glass. It is worth pointing out that in real-world applications PV film is supposed to be applied in place of the solar control film, i.e. on face 2 of the window (the internal side of the external pane). So, energy production is not affected and, at the same time the remaining layers of the window construction may be arranged depending on climate conditions and national regulations.

Table 5.
Material properties used in Daysim calculations

Material	*Colour*	*Reflectance [%]*	*Transmissivity [%]*	*Specularity [%]*	*Roughness [%]*
Indoor flooring	Stone grey	20.0	0.00	0.70	1.00
Internal walls	Beige 2k208	60.0	0.00	0.00	0.00
Indoor ceiling	White	80.0	0.00	0.00	0.00
Clear glass	Neutral	-	79.1	-	-
PV Pero-glass	Neutral	-	38.1	-	-

Default settings were used in all cases. Although Daysim could also be used to estimate the annual use of electric energy for artificial lighting, this calculation was done using a Matlab script that, using Daysim output, was able to compute the yearly electric energy request per unit area. This choice was made to account for the significant depth of the offices, that suggested a two-zone subdivision of the artificial lighting should be employed. In this way, artificial lighting was turned on in each portion only when the

Post-print version of the paper published in Applied Energy, Volume 205, 1 November 2017, Pages 834-846, doi: https://doi.org/10.1016/j.apenergy.2017.08.112

average illuminance over the relevant sensors fell below the threshold. The minimum threshold to turn on the light in the reference office was set to 500 lx, while the installed power density was set to 10.66 W/m^2. [48] The analysis was carried out for each orientation. Finally, as there are a number of areas in the building with no daylighting (mostly technical and service spaces, and corridors), they were given an installed power density of 4.84 W/m^2, [48] and the light was assumed to be always on during office hours.

2.5 Effect of urban context on BIPV production

To investigate the effect of an urban context on BIPV energy yield, the previous analyses were repeated assuming the building was surrounded by buildings having the same height (12 m), and located at a distance of 15 m from each façade (Fig. 5). Default values (0.2) of diffuse reflectance were used for the shading surfaces of the buildings. Calculations were carried out in EnergyPlus using the FullExterior algorithm.

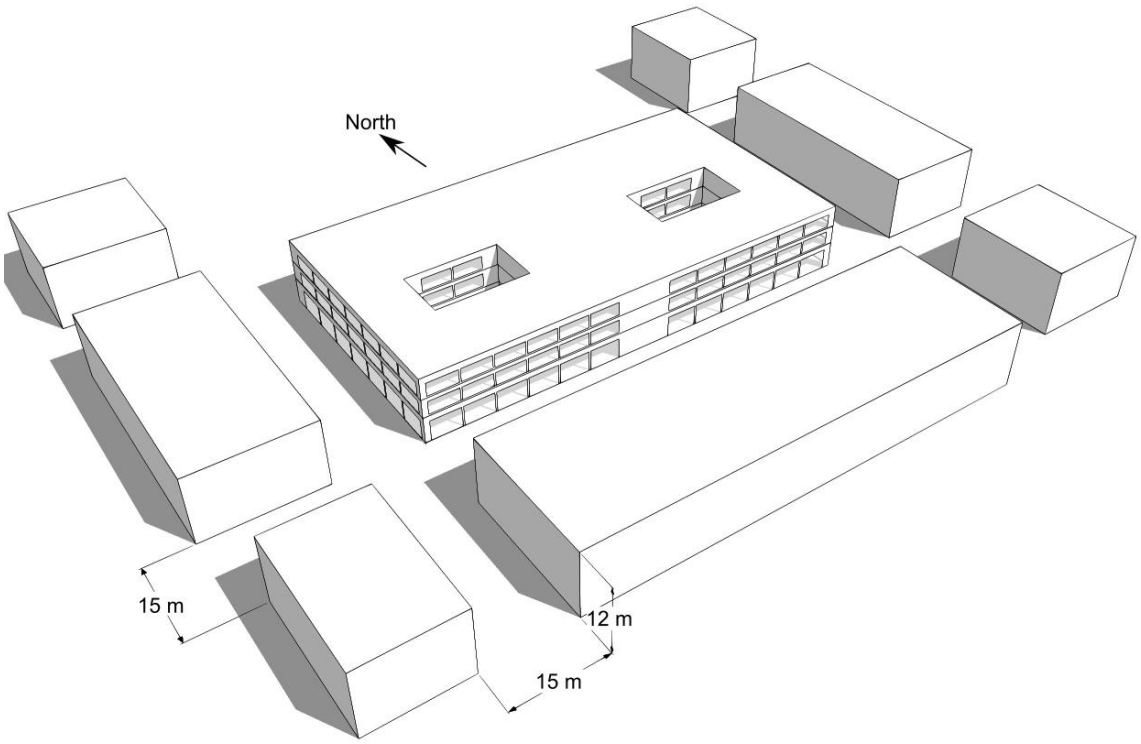

Fig. 5. *Outline of the 3D model used to investigate the effect of context on the energy yield of BIPV system*

Post-print version of the paper published in Applied Energy, Volume 205, 1 November 2017, Pages 834-846, doi: https://doi.org/10.1016/j.apenergy.2017.08.112

3 Results

3.1 Energy balance due to heating and air conditioning

Firstly, we consider the impact the addition of the PVs has in a passive state, without generating power, on the building's requirements. The thermal simulations on the whole building showed (Table 6) that the addition of the semitransparent (non-PV) shading system caused a small reduction of 0.8% in the overall electricity consumption due to reduced cooling load. Addition of an opaque PV shading increased the reduction to 2.5%, resulting from a small increase in heating and lighting load and a bigger drop in cooling load. The introduction of a semitransparent PV layer within the windows had similar effects, causing a 4% reduction in overall consumptions. Finally, the combination of PV glass and opaque PV shades caused the most extreme variations (–47.7 MWh/year for cooling, +12.8 MWh/year for heating, and +21.3 MWh/year for lighting), with an overall reduction of 5.3%. So, even though some tradeoffs appear, it is important to point out that the overall "passive" effect of using BIPV technologies is nonetheless somewhat positive. Some apparently undesired effects, such as the significant increase in lighting consumptions, will be demonstrated to be necessary in order to ensure better visual comfort, as shown in Sec. 3.3.

Table 6.
Comparison of electricity consumptions due to heating, cooling, and lighting under the different configurations analyzed. Other electric equipment loads are not included in the analysis as not related to proposed modifications. Acronyms as listed in Table 2.

	Electricity consumption [MWh/year]				
	CG	CG_S	CG_SPV	PV	PV_SPV
Heating electricty consumption	38.3	39.0	40.0	49.1	51.1
Cooling electricity consumption	170.1	166.6	160.0	133.3	122.4
HVAC electricity consumption	208.4	205.6	200.0	182.4	173.5
Lighting electricity consumption	42.0	42.9	44.3	58.5	63.3
Overall variable electricity consumption	250.4	248.5	244.3	240.5	237.2
Variation		-0.8%	-2.5%	-4.0%	-5.3%

Post-print version of the paper published in Applied Energy, Volume 205, 1 November 2017, Pages 834-846, doi: https://doi.org/10.1016/j.apenergy.2017.08.112

3.2 Energy produced by BIPV system

We now add in the further benefit of the PVs generating power. As shown in Table 7, the use of PV film over the entire glazed surface of East, South, and West facades (an area of about 1100 m^2) returned in total 27.9 MWh/year of electricity. This corresponds to 48% of the lighting energy demand, to 16% of the HVAC electricity demand, or to 12% of the overall electricity demand. In presence of the additional oqaque PV shades, a significant reduction of about 42% of the energy yield from the window glazing appeared, resulting in 16.3 MWh/year for the semi-transparent glazing. However, the PV shades themselves (total area of 340 m^2) provided an additional 25.7 MWh/year, resulting in an overall 42.0 MWh/year. This figure corresponds to an encouraging 66% of the lighting electricity demand, to 24% of the HVAC electricity demand, or to 18% of the overall electricity demand (excluding appliances).

Table 7
Comparison of annual electricity yield [MWh/year] due to PV panels integrated in glazing and shading systems.

			PV glass	PV glass, w/ Horiz. Shades				Horiz. Shades	
	East	South	West	East	South	West	East	South	West
Ground floor	2.51	7.13	2.68	1.75	4.44	1.86	1.65	5.62	1.59
1st & 2nd floor	1.65	4.35	1.77	0.96	2.12	1.03	1.65	5.19	1.59
Overall	5.81	15.82	6.22	3.68	8.69	3.92	4.95	15.99	4.77
Grand total [MWh/year]			27.9			16.3			25.7

However, it cannot be neglected that the application of the shading devices is not in reality a cost-effective action as it almost halved the energy output of the semi-transparent PV films. So, this suggests that under real-world conditions in which such treatments will have a cost, a better optimization of horizontal and vertical BIPV systems will be necessary – for example, windows directly beneath the shades may not have any glazing installed in the optimal case.

3.3 Visual comfort and lighting consumptions

Visual comfort assesments are an additional important metric to consider when implementing these systems. As detailed in Table 6, using PV film alone or in combination with the shades caused an increase in lighting electricity demand spanning

Post-print version of the paper published in Applied Energy, Volume 205, 1 November 2017, Pages 834-846, doi: https://doi.org/10.1016/j.apenergy.2017.08.112

from 39% to 50%. This result taken alone might discourage its usage, but the analysis of visual comfort parameters suggests that there are actually substantial advantages derived from its use. First, UDI was considered. As shown in Fig. 6, when the CG configuration was used, 50% of the points in the room had a "good" UDI, meaning that illuminance was within the optimal range for more than 50% of the working time. Adding the transparent shades increased the percentage of "good" conditions to 52.8%, while using PV film raised this percentage to 77.8%. The combined use of PV film and PV shades raised the percentage of acceptable UDI to 87.5%. Using only PV shades decreased the amount of points with "good" UDI to 59.7%.

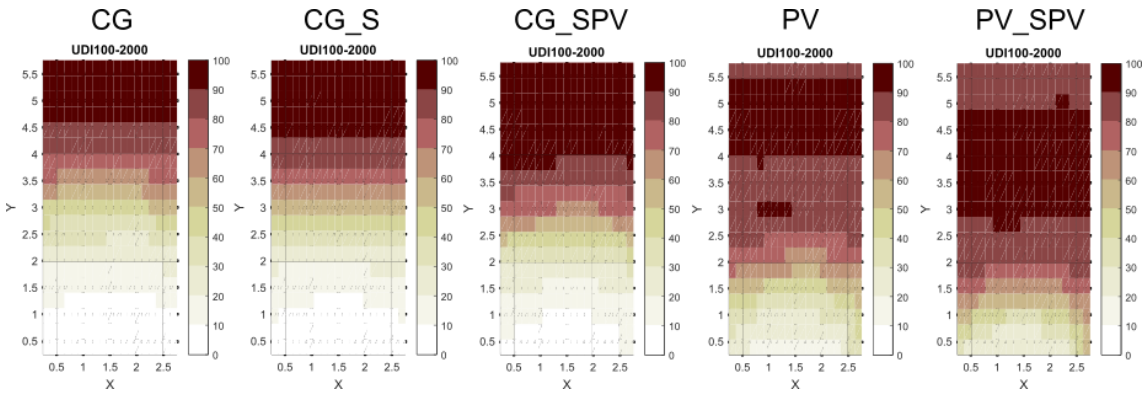

Fig. 6. *Spatial distribution of the percentage of time during the work year in which the Useful Daylight Illuminance (UDI) is within comfort limits for the selected locations. Acronyms as listed in Table 2. X and Y represent the test-room dimensions, expressed in m.*

The effectiveness of building-integrated perovskite cells was also demonstrated in terms of glare reduction. The same set of data used for UDI was adopted for DGP, allowing a clear comparison between all the design solutions proposed in this work.

As shown in Fig. 7, a dramatic glare attenuation was attained on the south-exposed facade, on a yearly distribution, when passing from a simply shaded glazing (current state) to the case employing semitransparent glazing and a high performing PV shading as well. An even more impressive improvement is derived from the combined use of PV film and PV shades, allowing the reference office to only have 17% of the working hours (over an entire year) above the 0.4 limit, due to high illuminance.

Post-print version of the paper published in Applied Energy, Volume 205, 1 November 2017, Pages 834-846, doi: https://doi.org/10.1016/j.apenergy.2017.08.112

The most significant variance was observed at hours close to noon: this is due to exposure of the window to the South. Similar advantages were found (although at different times of the day), when East and West exposures are considered.

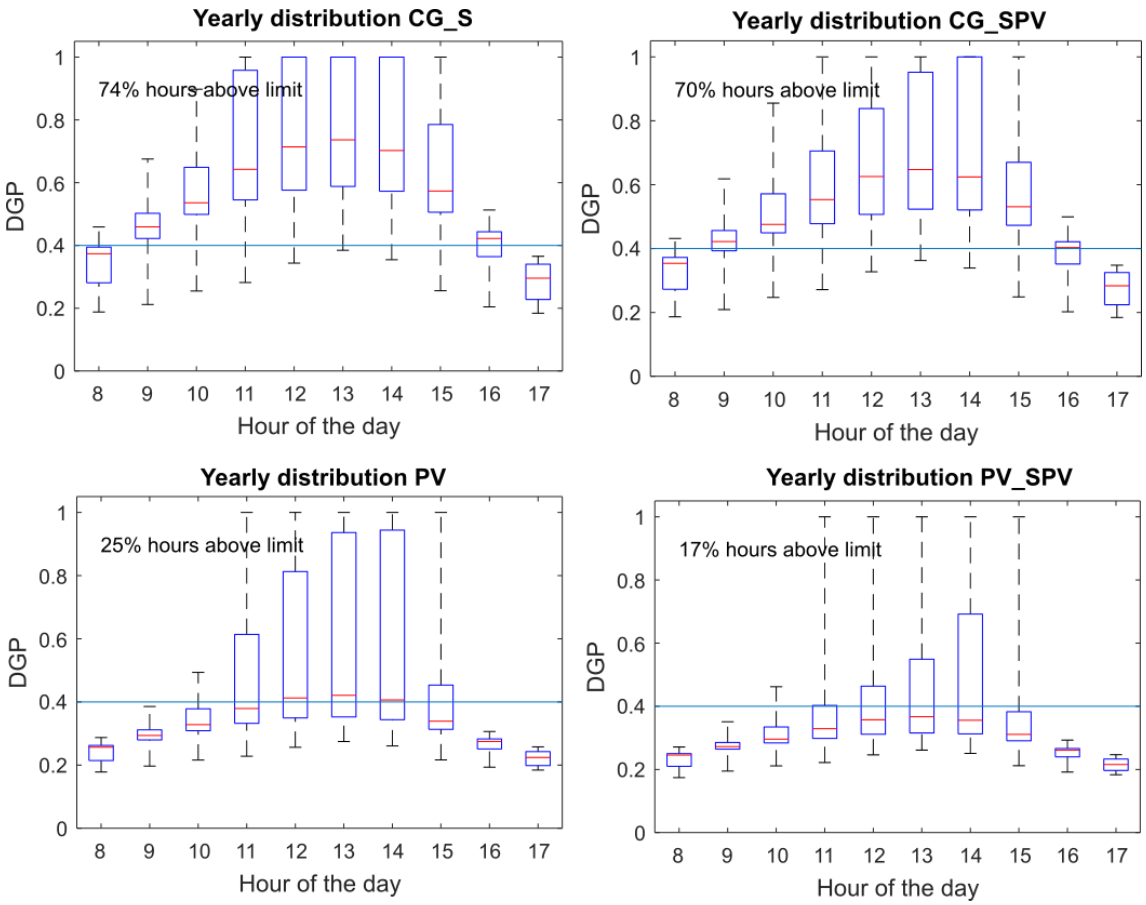

Fig. 7. *Boxplot of the Daylight Glare Probability (DGP) yearly distribution as a function of working hours for configurations under analysis. Box represents 1st and 3rd quartiles with the median given by the red horizontal line. Whiskers correspond to minima and maxima in each set.*

The DGP value in the CG_S case showed both median and interquartile values largely above the reference value 0.4, for almost all the hours observed. Such a value is typically assumed to discern "tolerable" values from "perceptible" glare conditions. Thus, the current state of the case-study building shows relevant shortcomings in terms of visual comfort indoor, since 74% hours are definitely above the reference limit. The yearly distribution showed just a small improvement from employing clear glass shaded by means of opaque PV shadings (CG_SPV). The lower panels of Fig. 7 show the DGP profiles when semitransparent perovskite-based PV glazings were installed: only 25%

Post-print version of the paper published in Applied Energy, Volume 205, 1 November 2017, Pages 834-846, doi: https://doi.org/10.1016/j.apenergy.2017.08.112

hours exceeded the reference value, on an annual basis. Such a result was further improved when using PV glazing and PV shadings, with just 17% hours exceeding the limit. Furthermore, the use of PV glass and of opaque PV shadings resulted in a significant reduction of median and of quartile range with respect to the first two design solutions. Though in the PV case median values slightly overcame the reference value, this took place only between 12:00 AM and 1:00 PM. The best performing solution, in terms of effective glare attenuation was represented by the combination of PV glazings and PV shades.

3.4 Effect of surroundings and obstructions

To analyze the effect of surroundings and obstructions on semi-transparent PV glazings, Table 8 shows the energy yield per unit area as a function of the different configurations under investigation. First of all, it is important to point out that no significant variation appears among different floors when no obstructions are involved. The south façade performs better, yielding 30.5 kWh/m^{2}year, while east and west facades yield about one-third less energy. As already observed, the presence of the shades negatively affects the energy production, with a milder impact on the ground floor because of the larger dimension of the windows that minimizes the effect of cast shadows. Slight differences appear between first and second floor because shades on the second floor may cast shadows on the first floor windows.

The effect of surroundings is particularly evident at the ground floor where further reductions in energy yield appeared. To analyse the impact of surrounding buildings, results for the isolated were taken as a reference (Fig. 8) and comparisons were made between homogenous conditions (with/without shades) and for different exposure (East, South, West) and floor level (ground, first and second floor, respectively). Results for East and West facades were very similar and were consequently shown together. Predictably, ground floor surfaces were much more affected by the context, with the East/West glazings yielding 55% and 64% less energy, for the configurations without and with shades, respectively. South exposure experienced slightly lower reductions, corresponding to 48% and 58% less energy, without and with shades respectively. The

Post-print version of the paper published in Applied Energy, Volume 205, 1 November 2017, Pages 834-846, doi: https://doi.org/10.1016/j.apenergy.2017.08.112

reduction for the horizontal shades was about 10% for the East/West exposure, while yield for shades on the South facade dropped by only 2%.

Table 8.
Yearly energy yield per surface area of vertical semi-transparent PV windows with and without shading systems, as a function of urban context. Disaggregated data pertaining to different exposures (E=East, S=South, W=West) and floors (0=ground, 1=fist, 2=second).

	Yearly energy yield per unit area [kWh/m2]								
Exposition	E0	E1	E2	S0	S1	S2	W0	W1	W2
Isolated bldg no shades	19.9	19.9	19.9	30.5	30.5	30.5	21.3	21.3	21.3
Isolated bldg shades	13.9	11.7	12.8	19.1	15.0	15.1	14.8	12.5	13.7
Urban, no shades	9.0	13.4	17.5	15.7	24.3	28.1	9.4	14.3	18.7
Urban, shades	5.0	6.6	10.7	7.9	11.1	13.6	5.3	7.1	11.4

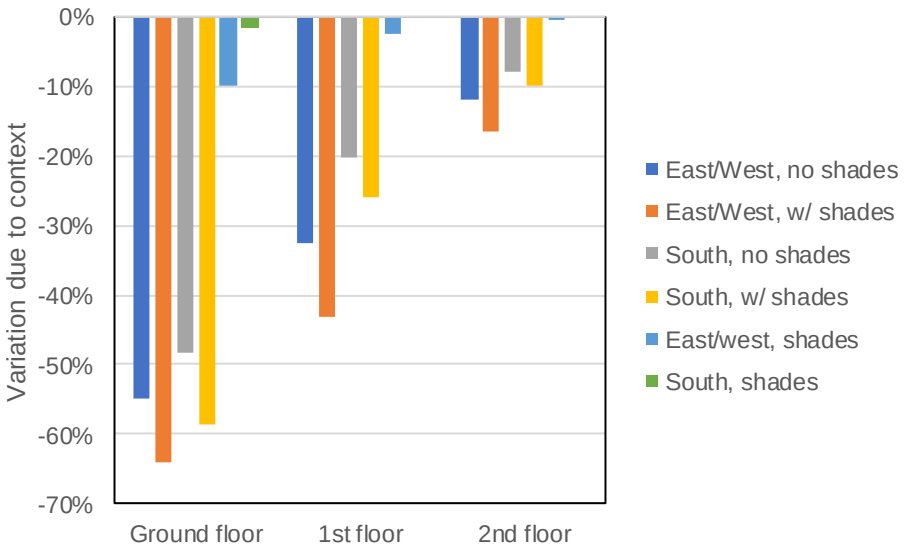

Fig. 8. *Outline of the percent variation due to urbanized context on the energy yield per surface unit. Results given as a function of floor, façade orientation, and presence of shades.*

The yield reduction for PV elements at the first floor was less severe. Again, East/West exposures suffered the most, with a 43% and 33% drop, respectively with and without shades. On the South facade the drop in energy yield was 26% and 20%, respectively with and without shades. For the horizontal shades, the performance drop appeared only on the East/West exposure, and was limited to a 2%.

Finally, surfaces on the second floor were only marginally affected by the context. The variation was between 8% and 17%, confirming the trends already observed. A detailed

Post-print version of the paper published in Applied Energy, Volume 205, 1 November 2017, Pages 834-846, doi: https://doi.org/10.1016/j.apenergy.2017.08.112

analysis showed that such decrease was mostly due shadows cast when the sun is close to the horizon.

Table 9 shows how the above considerations affected the overall electric energy yield due to PV panels integrated in façade glazing and horizontal shading systems, also reporting the overall yield variation when considering the building in ideal isolated conditions and in an urban context. The maximum overall energy yield was achieved for the isolated building with PV shades (42.3 MWh/year), which was reduced to 33 MWh/year when the building was considered to be in the presence of adjacent buildings. The maximum variation due to urban surroundings (–42%) was observed for the vertical PV glazing, when shades were adopted. Such variations reached the most significant values at the ground floor, either with (–61%) and without shades (–51%). The lowest yield change was reported for the second floor: –10% for the urban context when no shades were employed and –13% with shades.

Table 9.
Overall variation of electricity yield due to PV panels integrated in glazing and shading systems when the building is located in an urban context. Disaggregated data pertaining to vertical surfaces (Vert), Horizontal shades (Hor), and to overall surfaces located at different floors are also given.

	Yearly Energy yield [MWh/year]					
Exposition	Overall	Vert	Horiz	Grnd Floor	1st Floor	2nd Floor
Isolated bldg no shades	27.9	27.9		12.3	7.8	7.8
Isolated bldg shades	42.3	16.6	25.7	8.1	4.2	4.3
Urban, no shades	18.8	18.8		6.0	5.8	7.0
Urban, shades	33.0	9.7	23.4	3.2	2.7	3.8
Variation, no shades	-33%	-33%		-51%	-26%	-10%
Variation, shades	-22%	-42%	-9%	-61%	-34%	-13%

The presence of an urban context around the building not only affected the PV energy yield, but is likely to change the whole energy balance of the building due to a predictable reduction in cooling loads, and an increase in heating and lighting loads. Similarly, visual comfort may benefit from the presence of neighboring buildings which may prevent direct sunlight from entering the offices. Just to give a numerical value, a Daysim simulation of a typical office (under the CG reference condition) on the first floor and approximately located at the center of the South facade, returned 54% of the working hours above the

Post-print version of the paper published in Applied Energy, Volume 205, 1 November 2017, Pages 834-846, doi: https://doi.org/10.1016/j.apenergy.2017.08.112

critical DGP value. A comparison with the results given in Figure 8 clearly shows the improvement. Even greater advantages are expected at ground floor. As a detailed analysis of all the energetic implications of the urban context would require a much lengthier discussion, it was not included at this stage.

4 Discussion

The complexity of the results reported above requires a holistic approach for a useful, coherent discussion. We wish to identify the best compromise for an ideal choice, in terms of costs, energy yield, exploitation of daylighting and glare attenuation, by relating the energy yield reported for the different design solutions with the outputs of the daylighting performance.

Table 6 clearly showed that either PV or PV_SPV design solutions reported the most impressive reduction of electricity consumptions (for HVAC, cooling and overall variable electricity loads). Nevertheless, when shadings were adopted, the energy yield of building integrated semitransparent perovskite cells on glazings was almost halved (-42%) and an increase of energy consumption for artificial lighting was observed, due to the use of PV on glazings and shadings as well. On the other hand, visual comfort analysis supported the idea that simultaneous use of both technologies may be advantageous (neglecting costs), since daylight performances are significantly improved in the PV and PV_SPV scenarios. In addition, it should be noted that, given the unacceptable levels of over-illuminance and glare observed in all the configurations without PV glass, solar control glasses or other similar technologies would be needed anyway for an enhancement of comfortable working conditions, resulting in increased electricity consumptions for lighting and installation costs, without any advantage in term of energy production.

To identify a cost-effective solution, a combination of the energy yield results with the output of visual comfort assessment (in terms of UDI and DGP) suggested that the most convenient design solution was represented by the bare semitransparent PV glazings. Adoption of horizontal PV shades with clear glass windows (CG_SPV) offers only a minor improvement on visual comfort compared to the CG condition (Figure 7), suggesting that further solar control devices (or films) should be needed.

Post-print version of the paper published in Applied Energy, Volume 205, 1 November 2017, Pages 834-846, doi: https://doi.org/10.1016/j.apenergy.2017.08.112

When considering the energy balance of the building within the urban context, the horizontal PV shades showed the lowest yield attenuation (–9%) because their performance was barely affected by the presence of adjacent buildings, especially in summer when Sun is high on the horizon. Under these conditions, adopting PV glazings on the ground floor would be likely be not worthwhile, as they suffer significant yield reductions due to shadows by adjacent buildings. For the same reason, use of solar control devices would become unnecessary on the ground floor because glare and over-illumination would be significantly reduced. Conversely, on the first and second floor the PV_SPV solution might be considered as a viable option because shadows by adjacent buildings are limited, and combined horizontal and vertical PV panels, located on different exposures, allow an ideal mix capable of gathering energy throughout the day..

When considering avoiding the use of semi-transparent PV on glazings which are significantly shaded, an interesting cost-effective solution could be represented by moving the shades down by 60 cm (as in the original design), and use semi-transparent PV film only in the top pane of the window. In this way only 370 m^2 of film would be used instead of 1100 m^2. However, in terms of electricity yield such reduced surface (23% of the original surface) would be able to return 6.4 MWh/year, which added to the 25.7 MWh/year of the horizontal shades may cover 13% of the overall electricity load.

A further option which is worth considering, at least to provide a reference, is the location of PV panels on the top of the building. This layout was not considered from the beginning because the focal point of the paper was the use of innovative solutions based on semi-transparent cells, which could accelerate building integration of PV systems. However, considering the significant attenuation affecting PV modules on facades, due to mutual shading and due to surrounding buildings, combined with the large surface available on the rooftop, the latter solution is worth being briefly analyzed. As said, the available surface is about 3000 m^2, which is enough to ideally accommodate the 1100 m^2 plus the 340 m^2 of panels respectively used for semi-transparent glazings and for shades, leaving enough space for aisles and avoid mutual shading effects. On the rooftop, panels could be mounted assuming an ideal tilt angle, which at the latitude under investigation is about 34°. Under these conditions, using perovskite tandem cells, it is possible to gather 155

Post-print version of the paper published in Applied Energy, Volume 205, 1 November 2017, Pages 834-846, doi: https://doi.org/10.1016/j.apenergy.2017.08.112

kWh/(m^2 year), corresponding to 248 MWh/year for the whole surface. This result suggests that rooftop mounting is likely the best and most cost-effective solution, particularly for low-rise buildings located in urbanized areas. Nonetheless, facade-integrated solutions may represent a useful complement and, in the case of high-rise building, with limited presence of nearby buildings, may become really competitive compared to rooftop solutions. In addition, as shown in Fig. 9, neglecting absolute values, which clearly depend on the area covered by PV modules, façade integration offers a more stable energy yield, with higher values during early and late hours of the day compared to conventional rooftop location. This kind of output may better fit actual energy needs in an office, so the final choice as to the preferable location for PV modules, and whether they are semi-transparent or opaque, should be clearly evaluated case by case.

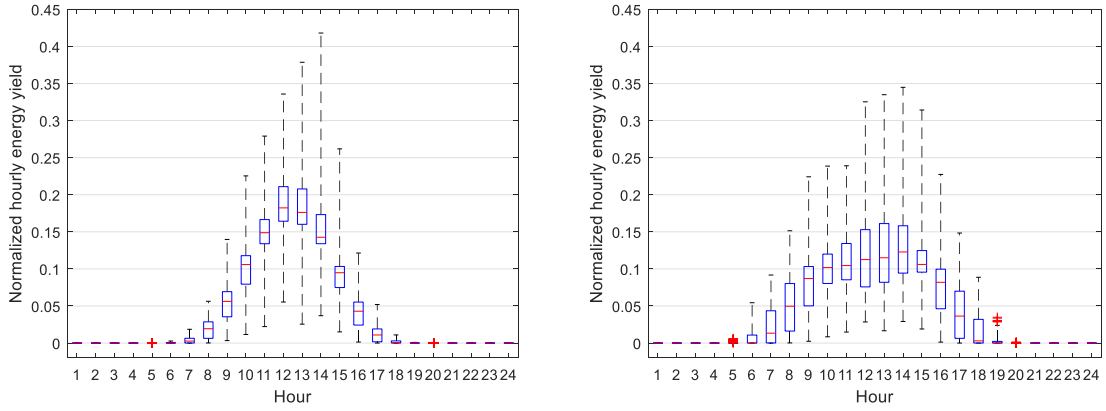

Fig. 9. *Boxplot of the yearly distribution of normalized hourly values of energy yield for(left) rooftop, ideal tilt PV modules, and (right) semi-transparent PV glazings averaged over E, S, and W exposures.. Normalization was carried out by dividing each hourly value by the overall daily energy. Box represents 1st and 3rd quartiles with the median given by the red horizontal line. Whiskers correspond to minima and maxima in each set.*

The energetic and visual comfort advantages demonstrated for building integrated perovskite-based cells should be taken into account without neglecting the other features of this innovative technology. Perovskites provide a very versatile PV solution - the room temperature solution processing of these cells, for instance, represents a chance for their low-cost scale-up. Moreover, they can be integrated not only in laminated glazings, as observed in crystalline solar cells, but they can be deposited on single glass panes.

Post-print version of the paper published in Applied Energy, Volume 205, 1 November 2017, Pages 834-846, doi: https://doi.org/10.1016/j.apenergy.2017.08.112

Consequently, they can be designed to be exploited on "face 2" in double glazing units, like for sputtered solar control films. Enhanced semitransparency by means of suitably tailored micro-islands, not visible to the naked eye is another strength of this versatile PV material: its spectrum (Figure 1) cannot be compared to any other PV technologies, with the same performances. Moreover, the inherent color neutrality of these films does not affect the spectral quality of filtered solar radiation, resulting in a strong compatibility with architectural glazing technology. Further considerations, based on recent scientific results of technoeconomic analyses for perovskite solar module manufacturing, undoubtedly corroborate the thesis of this manuscript. A quite complete assessment, in order to estimate manufacturing costs of perovskite-based solar modules was carried out by Chang et al. [49], who found values between 87 $/m^2 and 147 $/m^2. More recently, Song et al. [50] have calculated the direct manufacturing cost (31.7 $/m^2) and the minimum sustainable price (0.41 $/$W_p$) for a standard perovskite module operating with a conversion efficiency of 16%.

These values shows the potential of perovskite PV modules, although at a preindustrial stage. A comparison with manufacturing costs of other technologies is instructive: for instance, referring to the year 2013, a cost of 29 $/m^2 for CIGS cells and 27 $/m2 for CdTe cells was reported [50]. The good performance of perovskite cells is mainly due to lower cost of materials, lower energy needs and high material utilization. These considerations demonstrate that this novel technology could play a pivotal role in the roadmap to overcome the manifold market barriers still encountered by BIPV diffusion.

5 Conclusions

Following a previous study, where the potential benefits of using perovskite based BIPV solutions were investigated in a simplified ideal case, here a real building located in the suburban area of the city of Bari was considered. The building is characterized by a shape factor and by a relation with the surrounding buildings which may be considered typical of a large number of tertiary offices located in semi-industrial areas. Its internal distribution of small and medium offices is also typical of the Mediterranean area, so results obtained can be of interest for a much broader audience. Results showed that use of semi-transparent perovskite based PV glazing reduces the overall passive energy

Post-print version of the paper published in Applied Energy, Volume 205, 1 November 2017, Pages 834-846, doi: https://doi.org/10.1016/j.apenergy.2017.08.112

balance by 4%. In addition, 27.9 MWh/year can be obtained, resulting in a 15% net energy reduction compared to the reference condition. Adding horizontal PV shades predictably reduces the energy yield of the PV glazings (which drops to 16.6 MWh/yr), but returns an additional 25.7 MWh/year energy yield which combined to the passive benefits, returns a 22% net energy reduction compared to the reference case. In the presence of nearby buildings, cast shadows significantly reduced the energy yield. In particular, PV glazings on ground floor become mostly ineffective (the energy yield being reduced by more than 50%) and, from the visual comfort point of view, they do not contribute to reduce glare as direct sunlight is shaded by buildings. So, in terms of cost-optimal choices, use of PV glazings on ground floor would not be recommended in an urban area. PV shades are less detrimentally affected by the urban area, so they still represent an effective incorporation. At the top floor the drop in energy yield varies between 10% and 13% (depending on the presence of shades), but BIPV technologies remain a good choice. At the middle floor, energy yield reduction is in between, and adoption of optimized glazing combinations (e.g. to avoid mutual shading) becomes mandatory. Economic analysis carried out with reference to PV glazings showed that, assuming that a window replacement is required anyway, substituting a clear glass pane with a perovskite semi-transparent PV glass requires an extra investment with a 13 years pay back period. However, this value lowered to 5 years when assuming a solar control glass window as a baseline to compute extra costs. In fact, PV glass offers notable advantages in terms of visual comfort which could only be obtained by means of a solar control glass. Further investigations are certainly needed to better investigate the role played by building typology, shape factor, and surroundings on energy yield. However, our results here certainly point to the potential promise of perovskite-based BIPV for reducing building energy consumption in some cases.

Acknowledgments

This activity was partially funded by the Action Co-founded by Cohesion and Development Fund 2007-2013 – APQ Research Puglia Region “Regional programme supporting smart specialization and social and environmental sustainability – FutureInResearch”. G.E.E. is supported by the European Union’s Framework Programme

for Research and Innovation Horizon 2020 (2014-2020) under the Marie Skłodowska-Curie Grant Agreement No. 699935.

References

[1] Statistical Pocketbook 2014. Eur Union 2014. doi:10.2833/24150.

[2] Saifullah M, Gwak J, Yun JH. Comprehensive review on material requirements, present status, and future prospects for building-integrated semitransparent photovoltaics (BISTPV). J Mater Chem A 2016;4:8512–40. doi:10.1039/C6TA01016D.

[3] Gao T, Jelle BP, Ihara T, Gustavsen A. Insulating glazing units with silica aerogel granules: The impact of particle size. Appl Energy 2014;128:27–34. doi:10.1016/j.apenergy.2014.04.037.

[4] Jelle BP, Breivik C. The path to the building integrated photovoltaics of tomorrow. Energy Procedia 2012;20:78–87. doi:10.1016/j.egypro.2012.03.010.

[5] Heinstein P, Ballif C, Perret-Aebi LE. Building integrated photovoltaics (BIPV): Review, potentials, barriers and myths. Green 2013;3:125–56. doi:10.1515/green-2013-0020.

[6] Benemann J, Chehab O, Schaar-gabriel E. Building-integrated PV modules 2001;67:345–54.

[7] Mercaldo LV, Addonizio ML, Noce M Della, Veneri PD, Scognamiglio A, Privato C. Thin film silicon photovoltaics: Architectural perspectives and technological issues. Appl Energy 2009;86:1836–44. doi:10.1016/j.apenergy.2008.11.034.

[8] Zhang W, Lu L, Peng J, Song A. Comparison of the overall energy performance of semi-transparent photovoltaic windows and common energy-efficient windows in Hong Kong. Energy Build 2016;128:511–8. doi:10.1016/j.enbuild.2016.07.016.

[9] Lim JW, Lee SH, Lee DJ, Lee YJ, Yun SJ. Performances of amorphous silicon and silicon germanium semi-transparent solar cells. Thin Solid Films 2013;547:212–5. doi:10.1016/j.tsf.2013.03.038.

[10] Chae YT, Kim J, Park H, Shin B. Building energy performance evaluation of building integrated photovoltaic (BIPV) window with semi-transparent solar cells. Appl Energy 2014;129:217–27. doi:10.1016/j.apenergy.2014.04.106.

[11] Emmott CJM, Urbina A, Nelson J. Environmental and economic assessment of ITO-free electrodes for organic solar cells. Sol Energy Mater Sol Cells 2012;97:14–21. doi:10.1016/j.solmat.2011.09.024.

Post-print version of the paper published in Applied Energy, Volume 205, 1 November 2017, Pages 834-846, doi: https://doi.org/10.1016/j.apenergy.2017.08.112

[12] Tan H, Furlan A, Li W, Arapov K, Santbergen R, Wienk MM, et al. Highly Efficient Hybrid Polymer and Amorphous Silicon Multijunction Solar Cells with Effective Optical Management. Adv Mater 2016;28:2170–7. doi:10.1002/adma.201504483.

[13] O'Regan B, Grätzel M. A low-cost, high-efficiency solar cell based on dye-sensitized colloidal TiO2 films. Nature 1991;353:737–9.

[14] De Rossi F, Pontecorvo T, Brown TM. Characterization of photovoltaic devices for indoor light harvesting and customization of flexible dye solar cells to deliver superior efficiency under artificial lighting. Appl Energy 2015;156:413–22. doi:10.1016/j.apenergy.2015.07.031.

[15] Green MA, Ho-Baillie A, Snaith HJ. The emergence of perovskite solar cells. Nat Photonics 2014;8:506–14. doi:10.1038/nphoton.2014.134.

[16] Yang K, Li F, Zhang J, Veeramalai CP, Guo T. All-solution processed semi-transparent perovskite solar cells with silver nanowires electrode. Nanotechnology 2016;27:95202. doi:10.1088/0957-4484/27/9/095202.

[17] Zhang W, Anaya M, Lozano G, Calvo ME, Johnston MB, Miguez H, et al. Highly Efficient Perovskite Solar Cells with Tuneable Structural Color. Nano Lett 2015.

[18] Eperon GE, Stranks SD, Menelaou C, Johnston MB, Herz LM, Snaith HJ. Formamidinium lead trihalide: a broadly tunable perovskite for efficient planar heterojunction solar cells. Energy Environ Sci 2014;7:982. doi:10.1039/c3ee43822h.

[19] Martin A. Green, Keith Emery, Yoshihiro Hishikawa WW and EDD. Solar cell efficiency tables (Version 45). Prog Photovolt Res Appl 2015;23:1–9. doi:10.1002/pip.

[20] Best Research-Cell Efficiencies. Natl Renew Energy Lab 2016. www.nrel.gov/pv/assets/images/efficiency_chart. jpg.

[21] Gaspera E Della, Peng Y, Hou Q, Spiccia L, Bach U, Jasieniak JJ, et al. Ultra-thin High efficiency semitransparent perovskite solar cells. Nano Energy 2015;13:249–57. doi:10.1016/j.nanoen.2015.02.028.

[22] Eperon GE, Burlakov VM, Goriely A, Snaith HJ. Neutral color semitransparent microstructured perovskite solar cells. ACS Nano 2014;8:591–8. doi:10.1021/nn4052309.

[23] Hörantner MT, Nayak PK, Mukhopadhyay S, Wojciechowski K, Beck C, McMeekin D, et al. Shunt-Blocking Layers for Semitransparent Perovskite Solar Cells. Adv Mater Interfaces 2016:n/a-n/a. doi:10.1002/admi.201500837.

[24] Cannavale A, Eperon GE, Cossari P, Abate A, Snaith HJ, Gigli G. Perovskite photovoltachromic cells for building integration. Energy Environ Sci 2015;8:1578–84.

Post-print version of the paper published in Applied Energy, Volume 205, 1 November 2017, Pages 834-846, doi: https://doi.org/10.1016/j.apenergy.2017.08.112

[25] Cannavale A, Cossari P, Eperon GE, Colella S, Fiorito F, Gigli G, et al. Forthcoming Perspectives of Photoelectrochromic Devices: A critical review. Energy Environ Sci 2016;9:2682–719. doi:10.1039/C6EE01514J.

[26] Boyce P, Eklund N, Mangum S, Saalfield C, Tang L. Minimum acceptable transmittance of glazing. Light Res Technol 1995;27:145–52. doi:10.1177/14771535950270030201.

[27] Clarissa Zomer, André Nobre, Pablo Cassatella TR and RR. The balance between aesthetics and performance in building-integrated photovoltaics in the tropics. Prog Photovolt Res Appl 2007;15:659–76. doi:10.1002/pip.

[28] Yang RJ, Zou PXW. Building integrated photovoltaics (BIPV): Costs, benefits, risks, barriers and improvement strategy. Int J Constr Manag 2016;16:39–53. doi:10.1080/15623599.2015.1117709.

[29] Eke R, Senturk A. Monitoring the performance of single and triple junction amorphous silicon modules in two building integrated photovoltaic (BIPV) installations. Appl Energy 2013;109:154–62. doi:10.1016/j.apenergy.2013.03.087.

[30] Chatzipanagi A, Frontini F, Virtuani A. BIPV-temp: A demonstrative Building Integrated Photovoltaic installation. Appl Energy 2016;173:1–12. doi:10.1016/j.apenergy.2016.03.097.

[31] Peng J, Curcija DC, Lu L, Selkowitz SE, Yang H, Zhang W. Numerical investigation of the energy saving potential of a semi-transparent photovoltaic double-skin facade in a cool-summer Mediterranean climate. Appl Energy 2016;165:345–56. doi:10.1016/j.apenergy.2015.12.074.

[32] Cannavale A, Fiorito F, Resta D, Gigli G. Visual comfort assessment of smart photovoltachromic windows. Energy Build 2013;65:137–45. doi:10.1016/j.enbuild.2013.06.019.

[33] Favoino F, Fiorito F, Cannavale A, Ranzi G, Overend M. Optimal control and performance of photovoltachromic switchable glazing for building integration in temperate climates. Appl Energy 2016;178:943–61. doi:10.1016/j.apenergy.2016.06.107.

[34] Cannavale A, Hörantner M, Eperon GE, Snaith HJ, Fiorito F, Ayr U, et al. Building integration of semitransparent perovskite-based solar cells: Energy performance and visual comfort assessment. Appl Energy 2017;194:94–107. doi:10.1016/j.apenergy.2017.03.011.

[35] Oliver M, Jackson T. Energy and economic evaluation of building-integrated photovoltaics 2001;26:431–9.

[36] Giles E. Eperon, Tomas Leijtens, Kevin A. Bush, Rohit Prasanna, Thomas Green, Jacob Tse-Wei Wang, David P. McMeekin, George Volonakis, Rebecca L. Milot, Richard May, Axel Palmstrom, Daniel J. Slotcavage, Rebecca A.

Post-print version of the paper published in Applied Energy, Volume 205, 1 November 2017, Pages 834-846, doi: https://doi.org/10.1016/j.apenergy.2017.08.112

Belisle, Jay B. Patel, Elizabeth S. Parr HJS. Perovskite-perovskite tandem photovoltaics with optimized band gaps. Science (80-) 2016;354:861–5.

[37] Energy AS for EE and R. International Glazing Database 2011. https://windows.lbl.gov/materials/IGDB/.

[38] Avdelidis NP, Moropoulou A. Emissivity considerations in building thermography. Energy Build 2003;35:663–7. doi:10.1016/S0378-7788(02)00210-4.

[39] ASHRAE. International Weather for Energy Calculations (IWEC Weather Files) Version 2.0. Atlanta: ASHRAE; 2012.

[40] You J, Hong Z, Yang YM, Chen Q, Cai M, Song T, et al. Perovskite Solar Cells with High E ffi ciency and Flexibility 2014:1674–80.

[41] Energy UD of. EnergyPlus version 8.6 documentation, Engineering Reference. 2016.

[42] Reinhart CF, Walkenhorst O. Validation of dynamic RADIANCE-based daylight simulations for a test office with external blinds. Energy Build 2001;33:683–97. doi:10.1016/S0378-7788(01)00058-5.

[43] Jacobs A., Radiance Cookbook. (2014), available at: http://www.jaloxa.eu/resources/radiance/documentation/docs/radiance_cookbook.pdf (last visited 23/06/2017)

[44] Nabil A, Mardaljevic J. Useful daylight illuminance: a new paradigm for assessing daylight in buildings. Light Res Technol 2005;37:41–59. doi:10.1191/1365782805li128oa.

[45] Nabil A, Mardaljevic J. Useful daylight illuminances: A replacement for daylight factors. Energy Build 2006;38:905–13. doi:10.1016/j.enbuild.2006.03.013.

[46] Wienold J, Christoffersen J. Evaluation methods and development of a new glare prediction model for daylight environments with the use of CCD cameras. Energy Build 2006;38:743–57. doi:10.1016/j.enbuild.2006.03.017.

[47] Mardaljevic J, Andersen M, Roy N, Christoffersen J. Daylighting Metrics: Is There a Relation Between Useful Daylight Illuminance and Daylight Glare Probability? Ibpsa-Engl Bso12 2012:189–96.

[48] ASHRAE. Standard 189.1-2009 -- Standard for the Design of High-Performance Green Buildings (ANSI Approved; USGBC and IES Co-sponsored). Ashrae 2010. http://www.techstreet.com/ashrae/standards/ashrae-189-1-2009?product_id=1668986.

[49] Chang NL, Yi Ho-Baillie AW, Basore PA, Young TL, Evans R, Egan RJ. A manufacturing cost estimation method with uncertainty analysis and its application to perovskite on glass photovoltaic modules. Prog Photovoltaics Res Appl 2017;25:390–405. doi:10.1002/pip.2871.

Post-print version of the paper published in Applied Energy, Volume 205, 1 November 2017, Pages 834-846, doi: https://doi.org/10.1016/j.apenergy.2017.08.112

[50] Song Z, Mcelvany C, Phillips AB, Celik I, Krantz P, Watthage SC, et al. A technoeconomic analysis of perovskite solar module manufacturing with low-cost materials and techniques. Energy Environ Sci 2017;10:1297–305. doi:10.1039/C7EE00757D.

Post-print version of the paper published in Applied Energy, Volume 205, 1 November 2017, Pages 834-846, doi: https://doi.org/10.1016/j.apenergy.2017.08.112